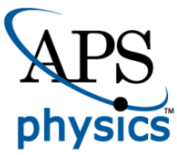

Fast control of topological vortex formation in Bose-Einstein condensates by counterdiabatic driving

Shumpei Masuda, Utkan Güngördü, Xi Chen, Tetsuo Ohmi, and Mikio Nakahara

Phys. Rev. A **93**, 013626 — Published 26 January 2016

DOI: 10.1103/PhysRevA.93.013626

Fast control of topological vortex formation in BEC by counter-diabatic driving

Shumpei Masuda,[1] Utkan Güngördü,[2] Xi Chen,[3] Tetsuo Ohmi,[4] and Mikio Nakahara[3,4]

[1] *James Franck Institute, The University of Chicago, Chicago, Illinois 60637, USA*
[2] *Department of Physics and Astronomy and Nebraska Center for Materials and Nanoscience, University of Nebraska, Lincoln, Nebraska 68588, USA*
[3] *Department of Physics, Shanghai University, 200444 Shanghai, People's Republic of China*
[4] *Research Center for Quantum Computing and Department of Physics, Kinki University, Higashi-Osaka, 577-8502, Japan*

Fast creation of a single vortex in BEC of alkali atoms at a prescribed position and time is still challenging even though various methods to create single and multiple vortices have been proposed and demonstrated. Topological vortex formation is advantageous in this respect over other methods in that the position and the time of vortex formation is highly controllable. This method requires inversion of the bias magnetic field along the axis of the condensate, which leads to unwanted atom loss due to non-adiabatic transitions when the bias field crosses zero. It is the purpose of this paper to propose a scheme that enables a fast creation of a vortex in much shorter time than needed for adiabatic control time by introducing the counter-diabatic field to avert the atom loss. We further introduce a gauge transformation so that the required magnetic field is generated by manipulating the current of the Ioffe bars, which makes our proposal experimentally feasible.

PACS numbers: 02.30.Yy, 37.90.+, 67.85.Fg, 03.75.Lm

I. INTRODUNCTION

Demonstration of quantized vortices in a superfluid is a manifestation of the nonvanishing order parameter. Topological structure of vortices often reflects the manifold of the order parameter space. It is, therefore, natural to seek for the method to experimentally demonstrate formation of vortices once BEC of alkali metal atoms has been realized. Topological methods of vortex formation, which utilize the spinor structure of the order parameter, have been proposed [1–7], and formations of vortices in BEC [8–14] as well as other topological defects such as a skyrmion [15, 16] and a monopole [17, 18] have been demonstrated by means of phase imprinting. Topologically created vortices inevitably have multiple winding number that can be controlled by specifying the hyperfine spin of BEC. This opened up a new research subject in BEC; instability of a vortex with a high winding number into several vortices with lower winding numbers [19–28]. Different methods to create BEC vortices have been proposed, such as the method with stirring of BEC by a laser beam [29], oscillatory perturbation of trapping potential [30, 31] and synthetic magnetic field [32]. Fast creation of a topological vortex beyond the adiabatic limit is challenging because of serious loss of atoms due to unwanted non-adiabatic transitions. We propose a fast and precisely controlled formation of a single vortex in BEC by driving the hyperfine spin using the magnetic field designed to restrain unwanted non-adiabatic transitions. This counter-diabatic vortex formation scheme manifests its efficiency in fast creation process with the manipulation time far shorter than the adiabatic limit. The necessary magnetic field can be generated by ordinary Ioffe bars, and no annular trapping potential nor optical plug is required in the creation process.

This paper is organized as follows. In Sec. II, we give a brief review on topological vortex imprinting to establish notation and convention. In Sec. III, we obtain the counter-diabatic field (CDF) to flip the hyperfine spin with speed beyond the adiabatic limit and introduce an approximation so that it is physically feasible. In Sec. IV, we solve the Gross-Pitaevskii equation with the magnetic field obtained in Sec. III to show much more atoms are kept in the trap after the vortex formation with very short inversion time, compared to those without CDF. In Sec. V, we introduce a gauge transformation acting on the hyperfine spin so that the control magnetic field can be implemented by a usual experiment setup without sacrificing the efficiency. Section VI is devoted to summary.

II. TOPOLOGICAL VORTEX IMPRINTING

In topological vortex formation process, hyperfine spin of the condensate is manipulated so that the vortex phase is imprinted as a Berry phase. Initially, a vortex-free condensate in the weak field seeking state (WFSS) is trapped in a quadrupole magnetic field in the xy-plane with a uniform bias field B_z along the z-axis and, subsequently, the bias field is linearly reversed from B_z to $-B_z$ adiabatically. Then a vortex with the winding number $2F$ is formed, where F is the quantum number of the hyperfine spin of the condensate. We assume the translational invariance of the BEC along the z-axis by following the original scheme developed in Ref. [2].

Consider an atom with hyperfine spin $\boldsymbol{F} = (F_x, F_y, F_z)$ at a position $\boldsymbol{r}$ at time t. When the atom is under an external magnetic field $\boldsymbol{B}(\boldsymbol{r}, t)$, the interaction Hamiltonian is given by

$$H_B(\boldsymbol{r}, t) = \gamma \boldsymbol{B}(\boldsymbol{r}, t) \cdot \boldsymbol{F}, \tag{1}$$

where $\gamma = \mu_B g_F$, μ_B is the Bohr magneton and g_F is the g-factor of the hyperfine spin F. We take $F = 1$ in the following for definiteness, for which $\boldsymbol{F}$ is the 3-dimensinal irreducible representaion of $\mathfrak{su}(2)$. For topological vortex formation, we consider a special form of $\boldsymbol{B}$, that is, $\boldsymbol{B}(\boldsymbol{r}, t) = \boldsymbol{B}_\perp(\boldsymbol{r}) + \boldsymbol{B}_z(t)$, where

$$\boldsymbol{B}_\perp(\boldsymbol{r}) = B'_\perp(x, -y, 0) \tag{2}$$

is the static quadrupole field in the Ioffe-Pritchard trap, for which $B'_\perp = d|\boldsymbol{B}_\perp|/dr$ is approximately constant, while

$$\boldsymbol{B}_z(t) = (0, 0, B_z(t)), \tag{3}$$

with

$$B_z(t) = \begin{cases} B_z\left(1 - \frac{2t}{T}\right), & 0 \le t \le T \\ -B_z, & t \ge T \end{cases} \tag{4}$$

Namely, $B_z(t)$ is linearly reversed during a time interval T and kept fixed after $t = T$. We show below that a phase with the winding number 2 is imprinted through this process.

For a given $\boldsymbol{B}(\boldsymbol{r}, t)$, the Hamiltonian (1) has three normalized eigenstates

$$\begin{aligned} |\mathrm{WFSS}\rangle &= \frac{1}{2B}\begin{pmatrix} (B - B_z)e^{2i\phi} \\ -\sqrt{2}B_\perp e^{i\phi} \\ B + B_z \end{pmatrix}, \\ |\mathrm{NS}\rangle &= \frac{1}{\sqrt{2}B}\begin{pmatrix} -B_\perp e^{2i\phi} \\ \sqrt{2}B_z e^{i\phi} \\ B_\perp \end{pmatrix}, \\ |\mathrm{SFSS}\rangle &= \frac{1}{2B}\begin{pmatrix} (B + B_z)e^{2i\phi} \\ \sqrt{2}B_\perp e^{i\phi} \\ B - B_z \end{pmatrix}, \end{aligned} \tag{5}$$

where $B = |\boldsymbol{B}(\boldsymbol{r}, t)|$ and ϕ is the azimuthal angle. The corresponding eigenvalues are $|\gamma|B$, 0, and $-|\gamma|B$, respectively, where $\gamma = -\mu_B/2$. The WFSS with the highest energy $|\gamma|B$ is the only state that can be magnetically trapped. Note that the relative phase between components in Eq. (5) is compleltely fixed by the condition that the condensate is initially a vortex-free WFSS [3].

The bias field $B_z(0)$ at $t = 0$ is taken much larger than the quadrupole field in the domain of interest so that $B_z(0) \gg |\boldsymbol{B}_\perp|$ holds throughout the condensate. With this choice, we find

$$|\mathrm{WFSS}(0)\rangle \simeq \begin{pmatrix} 0 \\ 0 \\ 1 \end{pmatrix}, \tag{6}$$

by putting $B \simeq B_z$. If the condensate is entirely made of the WFSS at $t = 0$, the configuration is vortex-free as remarked above. Subsequently B_z is linearly reversed during the interval T. At $t = T/2$, at which $B_z(T/2) = 0$, the WFSS takes the form

$$|\mathrm{WFSS}(T/2)\rangle = \frac{1}{2}\begin{pmatrix} e^{2i\phi} \\ -\sqrt{2}e^{i\phi} \\ 1 \end{pmatrix} \tag{7}$$

where we used the equality $B = |\boldsymbol{B}_\perp|$ at $t = T/2$. Later at $t = T$, the bias field is completely reversed so that $B_z(T) = -B_z$ and ignoring $\boldsymbol{B}_\perp$ we obtain

$$|\mathrm{WFSS}(T)\rangle \simeq \begin{pmatrix} e^{2i\phi} \\ 0 \\ 0 \end{pmatrix}. \tag{8}$$

Observe that a vortex with the winding number 2 has been formed at $t = T$.

Formation of a vortex in our scenario is understood from a slightly different viewpoint. The expectation value of the hyperfine spin vector $\langle \boldsymbol{F}(t)\rangle_{\mathrm{W}} \equiv \langle \mathrm{WFSS}(t)|\boldsymbol{F}|\mathrm{WFSS}(t)\rangle$ traverses a meridian of the Bloch sphere as t is changed from 0 to T, starting from the South pole and ending up with the North pole. Which meridian the vector traverses depends on the angle ϕ. It is easy to show

$$\begin{aligned} &\langle F_x(t)\rangle_{\mathrm{W}} = -\frac{B_\perp \cos\phi}{B}, \langle F_y(t)\rangle_{\mathrm{W}} = \frac{B_\perp \sin\phi}{B}, \\ &\langle F_z(t)\rangle_{\mathrm{W}} = -\frac{B_z}{B}. \end{aligned} \tag{9}$$

For example, a hyperfine spin with $\phi = 0$ traverses a meridian with $\phi = \pi$, while one with $\phi = \pi/2$ traverses a meridian with $\phi = \pi/2$. The solid angle subtended by these two meridians is π, giving the relative phase difference of π between these two hyperfine spins at $t = T$. This is regarded as the Berry phase acquired by the adiabatic change of the magnetic field [3, 8]. In this way, as one circumnavigates around the z-axis along a circle in the xy-plane, one observes that the phase of the order parameter changes by an amount 4π, resulting in a vortex with the winding number 2 [3, 8].

Figure 1 shows the trajectories of the combined magnetic field $\boldsymbol{B} = \boldsymbol{B}_\perp + \boldsymbol{B}_z$ and $\langle \boldsymbol{F}\rangle_{\mathrm{W}}$ at $\phi = 0$. For the parameters used in our numerical solution in Sec. IV, we obtain $|\boldsymbol{B}_\perp(\boldsymbol{r})|/B_z(0) \simeq 2.7 \times 10^{-4}$ at $r = a_{\mathrm{HO}}$, the harmonic oscillator length of the trap. For such a small ratio, the trajectory of $\boldsymbol{B}$ completely overlaps with the vertical axis. For this reason, the ratio is changed to 0.1 in the figure for purposes of illustration. Observe that $\langle \boldsymbol{F}\rangle_{\mathrm{W}}$ is always antiparallel to $\boldsymbol{B}$.

A drawback of this scenerio is that the gap among WFSS, NS and SFSS disappears at $r = 0$ when $t = T/2$. This means that atoms at $r \simeq 0$ flip to NS and SFSS (the Majorana flops) when $t \sim T/2$ and escape from the trap. In fact, the numerical analysis made in [3] shows that there is an optimal $T = T_{\max}$ that gives the maximum number of atoms at $t = T$. If $T < T_{\max}$, atoms are lost due to non-adiabatic transitions while if $T > T_{\max}$, the condensate spends a long time while the gap is small and atoms are lost through slow passage of the small gap region. It is the purpose of the next section to prevent non-adiabatic transition by adding the counter-diabatic field and achieve fast formation of a vortex.

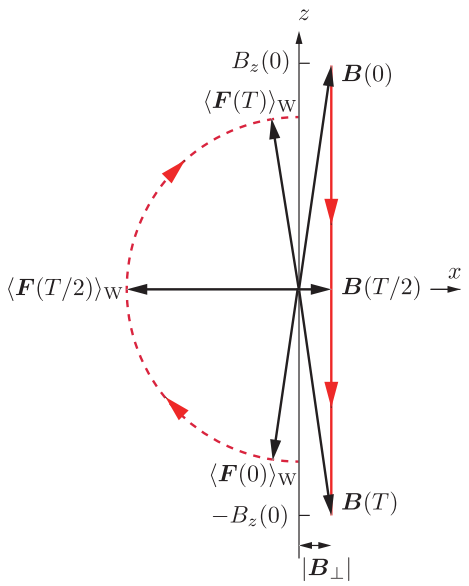

FIG. 1. (Color online) Trajectories of $\boldsymbol{B}$ (red line) and $\langle \boldsymbol{F}\rangle_{\rm W}$ (red dashed curve) of a hyperfine spin with $\phi = 0$. The vertical axis is the z-axis, while the horizontal axis is the x-axis. The quadrupole field is made unphysically large compared to $B_z(0)$ for purposes of illustration, see text. Vectors at $t = 0, T/2$ and T are explicitly shown.

III. COUNTER-DIABATIC FIELD

It is certainly desirable to have more atoms left in the trap after vortex formation. Control of atomic density in a wide range is essential to study the decay pattern of a vortex with a multiple winding number into several vortices with lower winding numbers [19–27, 33]. Keeping higher atom density after vortex formation is also indispensable to successful vortex pumping [5], which requires phase imprinting several times. In addition, it should be noted that higher atomic density implies (i) easier measurement of physical quantities, (ii) fighting against atom loss due to hyperfine spin changing collision and (iii) smaller vortex core size, which is advantageous for forming a vortex in an arbitrary position in the condensate [34].

Motivated by the concept of shortcuts to adiabaticity [35], we derive a control magnetic field for fast creation of a single vortex using the counter-diabatic formalism (or quantum transitionless driving) developed by Demirplak and Rice [36] and formulated by Berry [37, 38] and demonstrated experimentally in [39].

We briefly summarize the counter-diabatic approach to non-adiabatic quantum control. Let $H_0(t)$ be a time-dependent Hamiltonian and $|n(t)\rangle$ be an instantaneous eigenvector with the eigenvalue $E_n(t)$ such that $H_0(t)|n(t)\rangle = E_n(t)|n(t)\rangle$. In the adiabatic approximation, the solution to the time dependent Schrödinger equation is $|\psi_n(t)\rangle = e^{-i\gamma_n(t)}|n(t)\rangle$, where

$$\gamma_n(t) = \frac{1}{\hbar}\int_0^t dt' E_n(t') - i\int_0^t dt' \langle n(t')|\partial_{t'} n(t')\rangle. \quad (10)$$

Let $U(t) = \sum_n |\psi_n(t)\rangle\langle n(0)|$ be the time-evolution operator such that $U(t) : |n(0)\rangle \mapsto |\psi_n(t)\rangle$. The operator $U(t)$ defines a Hamiltonian $H(t) = i\hbar(\partial_t U(t))U^\dagger(t)$ for an arbitrary time evolution, not necessarily adiabatic, namely $|\psi_n(t)\rangle$ is the exact solution of

$$i\hbar\partial_t|\psi_n(t)\rangle = H(t)|\psi_n(t)\rangle, \quad (11)$$

where $|\psi_n(0)\rangle = |n(0)\rangle$ is satisfied by definition. If we write $H(t) = H_0(t) + H_{\rm CD}(t)$, the counter-diabatic Hamiltonian $H_{\rm CD}(t)$ is written as

$$H_{\rm CD}(t) = i\hbar\sum_n |\partial_t n(t)\rangle\langle n(t)|, \quad (12)$$

when the "parallel" condition, $\langle n(t)|\partial_t n(t)\rangle = 0$, is satisfied.

Let us apply the counter-diabatic scheme to our hyperfine spin system by taking H_0 and $|n\rangle$ as $H_0(\boldsymbol{r}, t) = H_B(\boldsymbol{r}, t)$ and the instantaneous eigenstates in Eq. (5), respectively. Note that the coordinate $\boldsymbol{r}$ here is just a parameter specifying the position of the atom in the condensate, and the geometric phase in Eq. (10) vanishes. By substituting Eq. (5) into Eq. (12), the counter-diabatic Hamiltonian is obtained as

$$H_{\rm CD} = \gamma \boldsymbol{B}_{\rm CD}\cdot\boldsymbol{F}, \quad (13)$$

where

$$\boldsymbol{B}_{\rm CD}(\boldsymbol{r}, t) = \frac{2\hbar}{\gamma T}\frac{B_z(0)B'_\perp}{B^2(r,t)}(y, x, 0) \quad (14)$$

is the CDF. Note that $\boldsymbol{B}_{\rm CD}$ is always orthogonal to $\boldsymbol{B}_\perp$. An important remark is in order here. When the counter-diabatic scheme is applied to a quantum system, it produces a counter-diabatic potential ($\gamma\boldsymbol{B}_{\rm CD}\cdot\boldsymbol{F}$ in our case) that prevents the quantum system from escaping from an adiabatic time evolution. There is no guarantee, however, that the counter-diabatic potential will be physically feasible. In fact, $\boldsymbol{B}_{\rm CD}$ in Eq. (14) does not satisfy div $\boldsymbol{B}_{\rm CD} = 0$. This is not unexpected since we did not consider the Maxwell equation while we derived $\boldsymbol{B}_{\rm CD}$. The way out of this problem is to fix the coordinate r to r_0 in $B^2(r, t)$ in the denominator of $\boldsymbol{B}_{\rm CD}(\boldsymbol{r}, t)$ so that $\boldsymbol{B}_{\rm CD}(r, t) \propto (y, x, 0)$ and div $\boldsymbol{B}_{\rm CD}$ vanishes. We numerically demonstrate below that the CDF in fact increases the number of atoms left in the trap after the vortex formation in a wide range of the inversion time T by using several values of r_0. $\boldsymbol{B}_{\rm CD}$ can be generated by four Ioffe bars that are obtained by rotating the confining Ioffe bars by an angle $\pi/4$ around the z-axis. We denote the combined magnetic field as $\bar{\boldsymbol{B}} = \boldsymbol{B} + \boldsymbol{B}_{\rm CD}$.

Before we close this section, we comment on the physical interpretation of $\boldsymbol{B}_{\rm CD}$. As $\boldsymbol{B}_z$ is reversed fast, atoms

in $|\mathrm{WFSS}\rangle$ in Eq. (5) "slip" to $|\mathrm{NS}\rangle$ and $|\mathrm{SFSS}\rangle$ by non-adiabatic transition if there is no CDF. $\boldsymbol{B}_{\mathrm{CD}}$, in a sense, "catches" those atoms so that their hyperfine spin state with respect to $\bar{\boldsymbol{B}}$ remains in $|\mathrm{WFSS}\rangle$ of Eq. (5) defined with respect to $\boldsymbol{B}$. It will be shown later in Figs. 3 and 10 that the total magnetic field with CDF bends asymmetrically from the meridian so that atoms enjoy being in $|\mathrm{WFSS}\rangle$ of Eq. (5) even with fast inversion of $\boldsymbol{B}_z(t)$. This is confirmed numerically in Sec. IV.

IV. TOPOLOGICAL VORTEX FORMATION WITH COUTER-DIABATIC FIELD

We numerically solve the Gross-Pitaevskii equation (GPE) with the designed magnetic field $\bar{\boldsymbol{B}}$;

$$i\hbar\partial_t\Psi_m(r,t) = \Big\{h_{mn} + g_n\delta_{mn}\sum_p|\Psi_p|^2 + g_s\sum_\alpha\sum_{l,p}\left(\Psi_l(F_\alpha)_{lp}\Psi_p\right)(F_\alpha)_{mn}\Big\}\Psi_n, \tag{15}$$

where $l,m,n,p\in\{-1,0,1\}$, $\alpha\in\{x,y,z\}$,

$$h_{mn} = \Big(-\frac{\hbar^2\nabla^2}{2M} - \mu\Big)\delta_{mn} + \mathcal{B}_{mn}, \qquad \mathcal{B} = \gamma\bar{\boldsymbol{B}}\cdot\boldsymbol{F}, \tag{16}$$

with the mass of the atom M, and the chemical potential μ (the eigenvalue of the GPE at $t=0$). Here g_n is the density-density coupling strength while g_s is the spin-spin coupling strength. To begin with, we need to find the initial condition to solve the GPE (15). Assuming that the initial hyperfine state is in the WFSS, $|\Psi(0)\rangle = f(\boldsymbol{r})|\mathrm{WFSS}(0)\rangle$, the order parameter is obtained by solving the stationary GPE

$$-\frac{\hbar^2}{2M}\Big[\frac{1}{r}\frac{d}{dr}\Big(r\frac{d}{dr}\Big) - \frac{\beta'^2}{2} - \frac{1}{4r^2}(7-8\cos\beta+\cos2\beta)\Big]f(r) + \gamma\bar{B}(r)f(r) + gf^3(r) = \mu f(r), \tag{17}$$

where $g = g_n + g_s$, $\bar{B}(r) = |\bar{\boldsymbol{B}}(\boldsymbol{r},0)|$,

$$\beta = \tan^{-1}\left[\frac{|\boldsymbol{B}_\perp(\boldsymbol{r}) + \boldsymbol{B}_{\mathrm{CD}}(\boldsymbol{r},0)|}{|\boldsymbol{B}_z(0)|}\right] \tag{18}$$

and $\beta' = d\beta/dr$. Here we note that $f(\boldsymbol{r})$ and $|\boldsymbol{B}_\perp(\boldsymbol{r}) + \boldsymbol{B}_{\mathrm{CD}}(\boldsymbol{r},0)|$ are in fact functions of r only.

The time-dependent GPE is solved numerically and we summarize the results below. Throughout our calculation, we have taken the parameters of ^{23}Na atoms [3]. The parameter set used is $M = 3.81\times10^{-26}$ kg, $g_n = 0.0378a_{\mathrm{HO}}^3\hbar\omega$, $g_s = 0$, $B_z(0) = 1$ G and $B'_\perp = 300$ G/cm, where $\omega = \hbar/(Ma_{\mathrm{HO}}^2)$ and $\hbar\omega \sim 3.49\times10^{-24}$ erg. The harmonic oscillator length is $a_{\mathrm{HO}} \sim 9.14\times10^{-1}$ μm. The time scale $\tau = 2\pi/\omega_L \sim 1.43$ μs is a reasonable measure of adiabaticity, where $\omega_L = \gamma|\bar{\boldsymbol{B}}(0,0)|/\hbar \sim 4.40\times10^6$ rad/s is the Larmor frequency at $r=0, t=0$. The chemical potential measured with respect to the Zeemen energy is found to be $\mu - \hbar\omega_L \sim 3.66\ \hbar\omega$. The number of atoms $N(0) = \iint_{-\infty}^{\infty}|\Psi|^2dxdy$ per unit length in the z-direction at $t=0$ is approximately 1.3×10^3 $\mu\mathrm{m}^{-1}$, where $|\Psi|^2 = \sum_p|\Psi_p|^2$. It turns out that $\boldsymbol{B}_{\mathrm{CD}}$ is negligibly small at $t=0$ and it can be ignored safely in solving Eq. (17). Figure 2 shows the time dependence of the ratio $|\boldsymbol{B}_{\mathrm{CD}}|/|\boldsymbol{B}_\perp|$ for $\log_{10}(T/\tau) = 1.4$ and $r_0/a_{\mathrm{HO}} = 2$, which is independent of r and depends only on t. Figure 3 shows schematics of $\boldsymbol{B}_\perp$ and $\boldsymbol{B}_{\mathrm{CD}}$ in the xy-plane. α_B is the angle between $\boldsymbol{B}_\perp$ and $\boldsymbol{B}_\perp + \boldsymbol{B}_{\mathrm{CD}}$ as defined in Sec. V.

We calculate the number of atoms left in the trap after the vortex formation takes place. To incorporate atom loss in the numerical simulation we multiply the order parameter by $h(r) = 0.5[1-\tanh((r-r_1)/\lambda)]$ with $r_1 = 30a_{\mathrm{HO}}$ and $\lambda = 2a_{\mathrm{HO}}$ at each time step of the

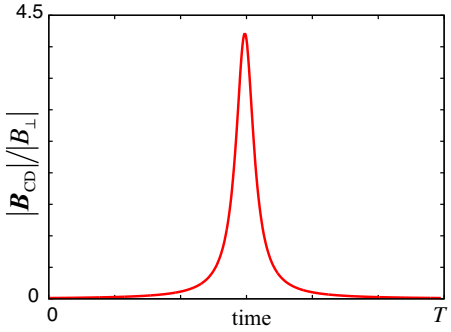

FIG. 2. (Color online) Time dependence of the ratio $|\boldsymbol{B}_{\mathrm{CD}}|/|\boldsymbol{B}_\perp|$, which is independent of r and depends only on t. Parameters are $\log_{10}(T/\tau) = 1.4$ and $r_0/a_{\mathrm{HO}} = 2$. For the parameters in the text, they amount to $T \sim 36$ μs and $r_0 \sim 1.83$ μm.

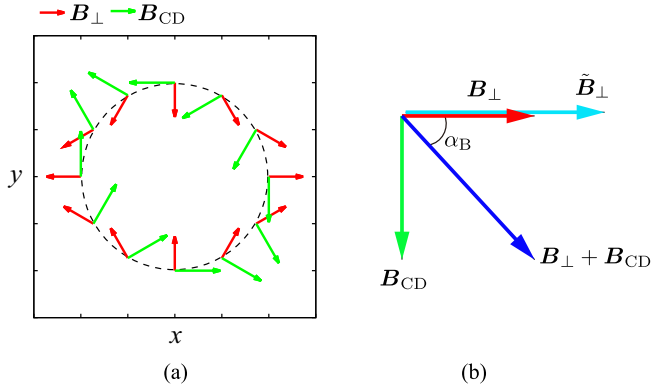

FIG. 3. (Color online) (a) Schematics of $\boldsymbol{B}_\perp$ (red arrow) and $\boldsymbol{B}_{\mathrm{CD}}$ (green arrow) in the xy-plane. (b) $\boldsymbol{B}_\perp$, $\boldsymbol{B}_{\mathrm{CD}}$ and $\boldsymbol{B}_\perp + \boldsymbol{B}_{\mathrm{CD}}$ (blue arrow) for $x>0$ and $y=0$. $\tilde{\boldsymbol{B}}_\perp$ (light blue arrow) is obtained by rotating $\boldsymbol{B}_\perp + \boldsymbol{B}_{\mathrm{CD}}$ by an angle α_{B} so that it is parallel to $\boldsymbol{B}_\perp$ (see Sec. V). Figures are conceptual and coordinates and magnetic fields are in arbitrary units.

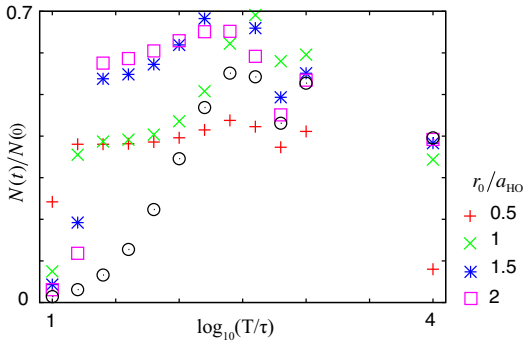

FIG. 4. (Color online) Fraction $N(t)/N(0)$ of atoms left in the trap long time after a vortex is formed. Since $t \gg T$, the condensate is in the pure WFSS. ∘ shows the fraction without $\boldsymbol{B}_{\rm CD}$ while other symbols show the fractions with $\boldsymbol{B}_{\rm CD}$ for different r_0. Here $\tau \sim 1.43$ μs.

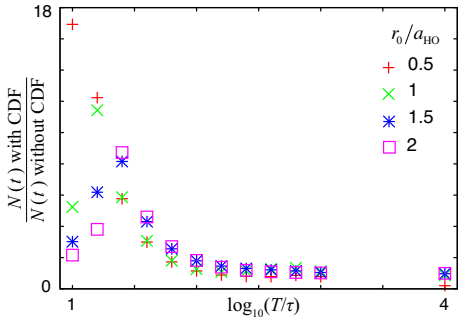

FIG. 5. (Color online) Ratio of $N(t)$ with the CDF to that without the CDF for $t \gg T$. The unit of time is $\tau \sim 1.43$ μs.

numerical simulation with the GPE (15) [3]. Figure 4 shows the fraction $N(t)/N(0)$ of atoms left in the trap at $t \gg T$. Most of the atoms left in the trap at t are in WFSS since t is large enough so that the SFSS and NS components are wiped out from the domain of interest by the action of $h(r)$. Since we replaced an unphysical $\boldsymbol{B}_{\rm CD}$ with a physical $\boldsymbol{B}_{\rm CD}$ satisfying div $\boldsymbol{B}_{\rm CD} = 0$, the result depends on the parameter r_0 in the denominator of Eq. (14). Observe the prominent improvement in the ratio $N(t)/N(0)$ for small T. This is more clearly seen by plotting $N(t)$ in the control with the CDF normalized by $N(t)$ in the control without the CDF. Figure 5 shows the ratios with the same r_0 as that in Fig. 4. The ratio reaches almost 20 for $T = 10\tau$ and $r_0 = 0.5a_{\rm HO}$.

Next, we show the CDF really suppresses the transitions WFSS → NS and WFSS → SFSS by looking at the projected atom numbers. For this purpose, we define the projection operators $\Pi_{\rm W} = |{\rm WFSS}\rangle\langle{\rm WFSS}|, \Pi_{\rm N} = |{\rm NS}\rangle\langle{\rm NS}|$ and $\Pi_{\rm S} = |{\rm SFSS}\rangle\langle{\rm SFSS}|$ and evaluate the amplitude of the order parameter (the number density) of respective hyperfine state

$$|\Psi_{\rm I}|^2 = \langle\Psi|\Pi_{\rm I}|\Psi\rangle, \tag{19}$$

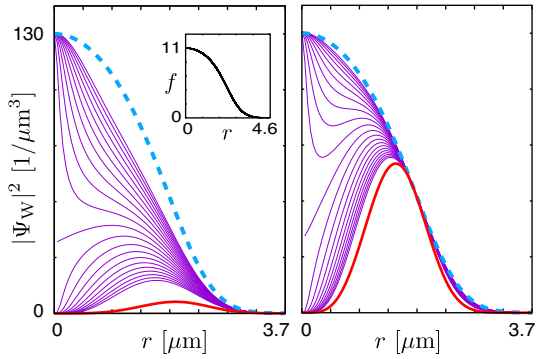

FIG. 6. (Color online) Snapshots of the amplitude of the order parameter $|\Psi_{\rm W}|^2$ are displayed in the left (right) panel for the control without (with) the CDF with the same parameter set as in Fig. 2. The thin purple curves are $|\Psi_{\rm W}|^2$ plotted sequentially at the same time interval for $T/2-\epsilon \le t \le T/2+\epsilon$ with $\epsilon = T/80$. The blue dashed curves and the red thick curves are $|\Psi_{\rm W}|^2$ at $t = 0$ and T, respectively. The inset is the profile of the condensate f at $t = 0$, which is obtained by solving Eq. (17) numerically. In the inset the units of r and f are μm and $\mu{\rm m}^{-3/2}$, respectively.

where $I = \{{\rm W}, {\rm N}, {\rm S}\}$, and the number of atoms per unit length of these states

$$N_{\rm I} = \iint dxdy|\Psi_{\rm I}|^2. \tag{20}$$

In the left (right) panel of Fig. 6 the snapshots of the amplitude $|\Psi_{\rm W}|^2$ are displayed for the control without (with) the CDF for the same parameter set as in Fig. 2. The amplitude $|\Psi_{\rm W}|^2$ is plotted sequentially with equal time interval for $T/2 - \epsilon \le t \le T/2 + \epsilon$ where $\epsilon = T/80$. The dashed blue curves and the thick red curves are $|\Psi_{\rm W}|^2$ at $t = 0$ and T, respectively. The inset shows the bound state order parameter $f(r)$ obtained by solving Eq. (17) for ^{23}Na. Vanishing order parameter at $r = 0$ and $t = T$ is a manifestation of the formation of a vortex in the WFSS. The results clearly show that more atoms are kept in the trap at $t = T$ with the CDF compared to the case without the CDF. It is also found that the amplitude in the region $r > 2$ μm does not change very much in the presence of CDF while considerable diminution takes place in the case without CDF. Observe that outstanding change in $|\Psi_{\rm W}|^2$ occurs only in the vicinity of $t = T/2$ at which B_z changes the sign. It turns out that the number of atoms in WFSS state is essentially constant for $t \ge T$ in both cases. Figure 7 shows the time dependence of $N_{\rm W}(t)/N(0)$ in the controls without CDF (dashed black curve) and with CDF (solid red curve) along with the ratios of other components. It is evident from this figure that transitions among states take place only at around $t = T/2$ and that non-adiabatic transition of WFSS at $t \sim T/2$ is greatly suppressed by CDF. This means that our approximation introduced in the denominator of (14) breaks down at $t \sim T/2$, when the original $\boldsymbol{B}_{\rm CD}$ in Eq. (14) diverges at $r = 0$. Otherwise, our simple approxi-

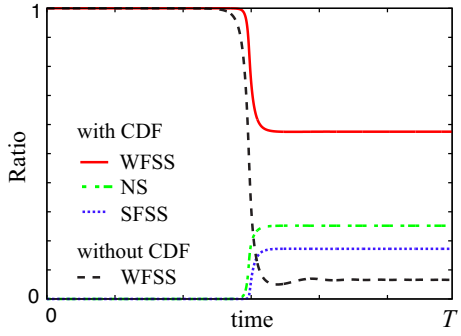

FIG. 7. (Color online) Instantaneous fraction of atoms $N_{\rm W}(t)/N(0)$ (red solid curve), $N_{\rm N}(t)/N(0)$ (green dashed curve) and $N_{\rm S}(t)/N(0)$ (blue dotted curve) with the CDF during the vortex formation for $\log_{10}(T/\tau) = 1.4$ and $r_0 = 2a_{\rm HO}$. The dashed black curve shows $N_{\rm W}(t)/N(0)$ without the CDF. Here $T \sim 36$ μs as before.

mation works reasonably well.

We repeat our analysis for a BEC with a larger number of atoms. Figure 8 shows the results for $f(0) = 20$ $a_{\rm HO}^{-3/2}$ corresponding to the density $\int\int_{-\infty}^{\infty} |\Psi|^2 dxdy \sim 2.1 \times 10^4$ μm^{-1} at $t = 0$. Figure 8(a) shows the fraction $N(t)/N(0)$ of atoms left in the trap at $t \gg T$ for various r_0. The black open circles are for the control without CDF. The fraction of the lost atoms without CDF is less than that for $f(0) = 10$ $a_{\rm HO}^{-3/2}$ shown in Fig. 4 since the initial wave function around $r = 0$ for $f(0) = 20$ $a_{\rm HO}^{-3/2}$ is flatter than that for $f(0) = 10$ $a_{\rm HO}^{-3/2}$ due to the positive coupling strength g. The CDF with $r_0 = 2.5a_{\rm HO}$ and $3a_{\rm HO}$ keep more atoms forming a vortex especially for small T. Figure 8(b) shows the ratios of $N(t \gg T)$ with the CDF to that without the CDF. Prominent improvement in the ratio is seen for small T.

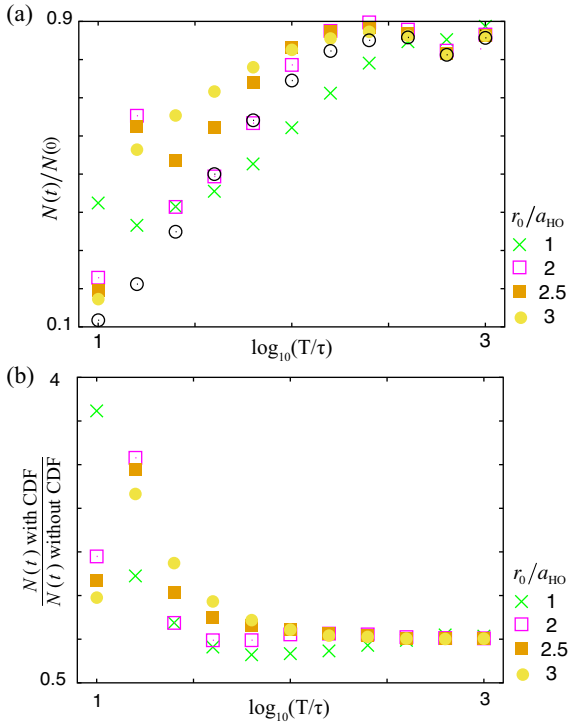

FIG. 8. (Color online) (a) Fraction $N(t)/N(0)$ of atoms left in the trap long time after a vortex is formed for $f(0) = 20$ $a_{\rm HO}^{-3/2}$ corresponding to $\int\int_{-\infty}^{\infty} |\Psi|^2 dxdy \sim 2.1 \times 10^4$ μm^{-1}. Since $t \gg T$, the condensate is in the pure WFSS. $\circ$ shows the fraction without $\boldsymbol{B}_{\rm CD}$ while other symbols show the fractions with $\boldsymbol{B}_{\rm CD}$ for different r_0. (b) Ratio of $N(t \gg T)$ with the CDF to that without the CDF.

V. MORE EXPERIMENTALLY FEASIBLE CONTROL

Now an important observation is in order. In our proposal in Sec. IV, we need to prepare two sets of Ioffe bars, one to produce the confining quadrupole field and the other to produce the CDF. Clearly this is demanding for experimentalists. All topological vortex formation experiments so far were conducted with a single confining magnetic field. Even if one could build a trap with two sets of Ioffe bars, aligning their centers exactly at the same place would be practically impossible. To circumvent this problem, we introduce time-dependent gauge transformation so that the combined field $\boldsymbol{B}_\perp + \boldsymbol{B}_{\rm CD}$ is rotated and the resulting field is parallel to the confining $\boldsymbol{B}_\perp$. Let

$$\alpha_B = \tan^{-1} \frac{|\boldsymbol{B}_{\rm CD}|}{|\boldsymbol{B}_\perp|} \tag{21}$$

be the angle between $\boldsymbol{B}_\perp + \boldsymbol{B}_{\rm CD}$ and $\boldsymbol{B}_\perp$ (see Fig. 3). If $\boldsymbol{B}_\perp + \boldsymbol{B}_{\rm CD}$ is rotated by α_B, it becomes parallel to $\boldsymbol{B}_\perp$ and hence it can be generated by a single set of Ioffe bars by controlling the current. This rotation is implemented by the unitary transformation

$$U(\alpha_B) = e^{-i\alpha_B F_z}. \tag{22}$$

Now the Zeeman term of the Hamiltonian is transformed as

$$U(\alpha_B)\gamma\bar{\boldsymbol{B}} \cdot \boldsymbol{F} U^\dagger(\alpha_B) = \gamma(\tilde{\boldsymbol{B}}_\perp + \boldsymbol{B}_z) \cdot \boldsymbol{F}, \tag{23}$$

where $\tilde{\boldsymbol{B}}_\perp = U(\alpha_B)(\boldsymbol{B}_\perp + \boldsymbol{B}_{\rm CD})U(\alpha_B)^\dagger \propto (x, -y, 0)$. Of course, this is not the whole story and there is a price we need to pay. The Hamiltonian in the rotating frame acquires a gauge term

$$-iU\partial_t U^\dagger = \dot{\alpha}_B F_z. \tag{24}$$

This term, proportional to F_z, works as a magnetic field in the z-direction and the bias field $B_z(t) = B_z(0)(1 - 2t/T)$ is replaced by

$$\tilde{B}_z(t) = B_z(0)\left(1 - \frac{2t}{T}\right) + \frac{\dot{\alpha}_B \hbar}{\gamma}. \tag{25}$$

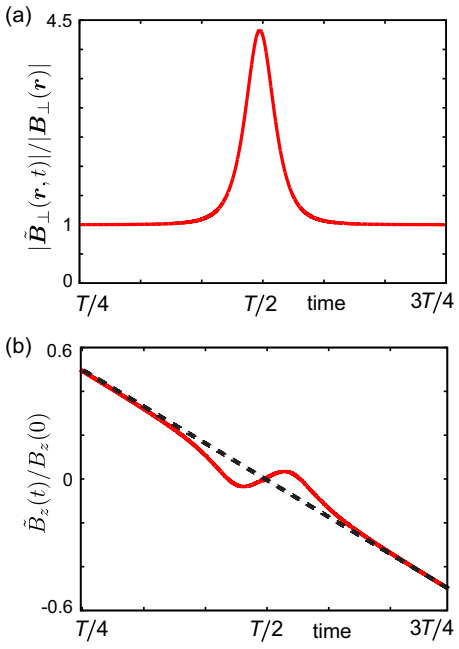

FIG. 9. (Color online) (a) $|\tilde{\boldsymbol{B}}_\perp(\boldsymbol{r},t)|/|\boldsymbol{B}_\perp(\boldsymbol{r})|$ and (b) $\tilde{B}_z(t)/B_z(0)$ (solid red curve) and $B_z(t)/B_z(0)$ (dashed black line) for the same parameters as those used in Fig. 7 with $T \sim 36$ μs. Deviations from the original fields $\boldsymbol{B}_\perp$ and $B_z(t)$ are promient only when $t \sim T/2$.

We denote the combined field as

$$\tilde{\boldsymbol{B}}(\boldsymbol{r},t) = \tilde{\boldsymbol{B}}_\perp(\boldsymbol{r},t) + \tilde{\boldsymbol{B}}_z(t), \tag{26}$$

where $\tilde{\boldsymbol{B}}_z(t) = (0,0,\tilde{B}_z(t))$. Note that α_B depends on time but not on space coordinates. Numerical caluculation shows that the number of atoms in WFSS at $t > T$ in the control with $\tilde{\boldsymbol{B}}(\boldsymbol{r},t)$ is exactly the same as that with $\bar{\boldsymbol{B}}(\boldsymbol{r},t)$ generated by two sets of Ioffe bars. Figure 9 shows $|\tilde{\boldsymbol{B}}_\perp(t)|/|\boldsymbol{B}_\perp|$ and $\tilde{B}_z(t)/B_z(0)$ for ^{23}Na with the parameters used in Fig. 7.

Figure 10 shows the schematic picture of the control magnetic field $\tilde{\boldsymbol{B}}$ obtained in this section. For $\phi = 0$, the modified magnetic field is always in the xz-plane, whose trajectory is shown in Fig. 10(a) and (b) in the solid red curve. Figure 10(b) also shows the trajectory of the control magnetic field $\bar{\boldsymbol{B}}$ obtained in Sec. IV and the trejectories of $\langle \boldsymbol{F}(t)\rangle_{\rm W}$ in both cases.

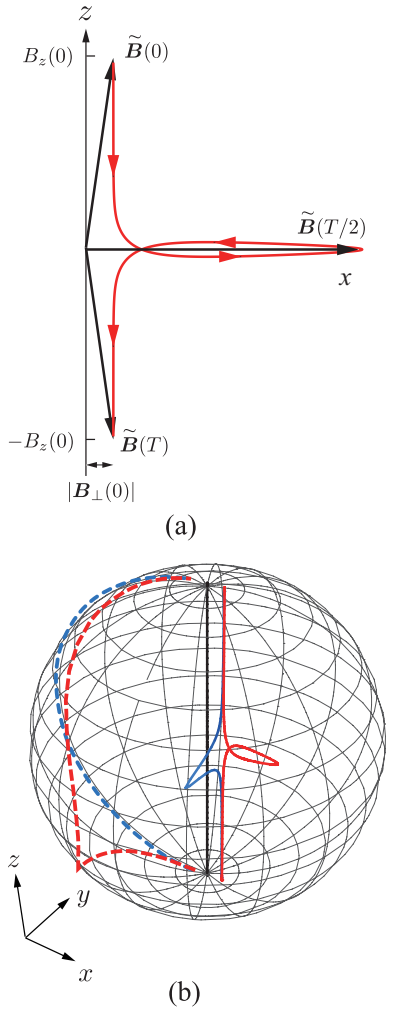

FIG. 10. (Color online) (a) Trajectory of $\tilde{\boldsymbol{B}}(\boldsymbol{r},t)$ for $\phi = 0$ is shown in a solid red curuve. The trajectory is in the xz-plane. (b) Trajectories of $\tilde{\boldsymbol{B}}(\boldsymbol{r},t)$ (the solid red curve), $\bar{\boldsymbol{B}}(\boldsymbol{r},t)$ (the solid blue curve), $\langle \boldsymbol{F}(t)\rangle_{\rm W}$ after the gauge transformation (broken red curve) and $\langle \boldsymbol{F}(t)\rangle_{\rm W}$ before the gauge transformation (broken blue curve). $|\boldsymbol{B}_\perp(0)|$ is taken unphysically large as in Fig. 1 for purposes of illustration. The vertical black line is the axis of the sphere and is given as a guide.

VI. SUMMARY

We have proposed a method to suppress non-adiabatic transitions while topological vortex formation takes place in BEC of alkali atoms. The counter-diabatic field is generated by a set of Ioffe bars, which is obtained by rotating the confining Ioffe bars, producing the confining quadrupole field, by $\pi/4$. Our numerical calculation demonstrates that non-adiabatic transitions are suppressed for any inversion time T and, in particular, suppression is most impressive for a small T. We can further improve this scheme by applying a gauge transformation to a rotating frame so that the combined field $\tilde{\boldsymbol{B}}_\perp$ is parallel to $\boldsymbol{B}_\perp$. Then, the control magnetic field can be generated with ordinary Ioffe bars by simply controlling the current. This also requires modulation of $B_z(t)$ from linear time-dependence. We believe our proposal is experimentally feasible by simple modifications of the existing setup.

Application of this work to vortex pumping [5] is in progress and will be reported elsewhere.

ACKNOWLEDGMENT

MN would like to thank Yuki Kawaguchi and Takeshi Kuwamoto for useful discussions. We are grateful to Tuomas Ollikainen, Mikko Möttönen and David S. Hall for discussions and interest in our work. The work of SM is partly supported by JSPS postdoc fellowship. UG is supported in part by the NSF under Grant No. Phy-1415600 and NSF-EPSCoR 1004094. XC's work is partially supported by the NSFC (11474193 and 61176118), the Shuguang and Pujiang Program (14SU35 and 13PJ1403000), the Specialized Research Fund for the Doctoral Program (2013310811003), the Program for Eastern Scholar. MN's work is supported in part by a "Topological Quantum Phenomena" Grant-in Aid for Scientific Research on Innovative Areas (No. 22103003) from the Ministry of Education, Culture, Sports, Science and Technology (MEXT) of Japan. MN, TO and UG are also grateful to JSPS for partial support from Grants-in-Aid for Scientific Research (Grant No. 26400422).

[1] M. Nakahara, T. Isohima, K. Machid, S.-I. Ogawa, and T. Ohmi, Physica B **284**, 17 (2000).

[2] T. Isoshima, M. Nakahara, T. Ohmi, and K. Machida, Phys. Rev. A **61**, 063610 (2000).

[3] S.-I. Ogawa, M. Möttönen, M. Nakahara, T. Ohmi, and H. Shimada, Phys. Rev. A **66**, 013617 (2002).

[4] M. Möttönen, N. Matsumoto, M. Nakahara, and T. Ohmi, J. Phys.: Condens. Matter **14**, 13481 (2002).

[5] M. Möttönen, V. Pietilä, and S. M. M. Virtanen, Phys. Rev. Lett. **99**, 250406 (2007).

[6] For a review, see V. Pietila, M. Möttönen and M. Nakahara, in *Electromagnetic, Magnetostatic, and Exchange-Interaction Vortices in Confined Magnetic Structures*, ed. by E. O. Kamenetskii, Transworld Research Network, 297 (2008).

[7] P. Kuopanportti, B. P. Anderson, and M. Möttönen, Phys. Rev. A **87**, 033623 (2013).

[8] A. E. Leanhardt, A. Görlitz, A. P. Chikkatur, D. Kielpinski, Y. Shin, D. E. Pritchard, and W. Ketterle. Phys. Rev. Lett. **89**, 190403 (2002).

[9] A. E. Leanhardt, Y. Shin, D. Kielpinski, D. E. Pritchard, and W. Ketterle, Phys. Rev. Lett. **90**, 140403 (2003).

[10] Y. Shin, M. Saba, M. Vengalattore, T. A. Pasquini, C. Sanner, A. E. Leanhardt, M. Prentiss, D. E. Pritchard, and W. Ketterle, Phys. Rev. Lett. **93**, 160406 (2004).

[11] M. Kumakura, T. Hirotani, M. Okano, Y. Takahashi, and T. Yabuzaki, Phys. Rev. A **73**, 063605 (2006).

[12] T. Isoshima, M. Okano, H. Yasuda, K. Kasa, J. A. M. Huhtamäki, M. Kumakura, and Y. Takahashi, Phys. Revl. Lett. **99**, 200403 (2007).

[13] T. Kuwamoto, H. Usuda, S. Tojo, and T. Hirano, J. Phys. Soc. Jpn. **79**, 034004 (2010).

[14] H. Shibayama, Y. Yasaku, and T. Kuwamoto, J. Phys. B: At. Mol. Opt. Phys. **44**, 075302 (2011).

[15] J. Y. Choi, W. J. Kwon, and Y. I. Shin, Phys. Rev. Lett. **108**, 035301 (2012).

[16] J.-y. Choi, W. J. Kwon, M. Lee, H. Jeong, K. An, and Y.-i. Shin, New J. Phys. **14**, 053013 (2012). Corrigendum, New J. Phys. **17**, 069501 (2015).

[17] M. W. Ray, E. Ruokokoski, S. Kandel, M. Möttönen, and D. S. Hall, Nature **505**, 657 (2014).

[18] M. W. Ray, E. Ruokokoski, K. Tiurev, M. Möttönen, and D. S. Hall, Science **348**, 544 (2015).

[19] M. Möttönen, T. Mizushima, T. Isoshima, M. M. Salomaa, and K. Machida, Phys. Rev. A **68**, 023611 (2003).

[20] Y. Kawaguchi and T. Ohmi, Phys. Rev. A **70** 043610 (2004).

[21] Y. Shin, M. Saba, M. Vengalattore, T. A. Pasquini, C. Sanner, A. E. Leanhardt, M. Prentiss, D. E. Pritchard, and W. Ketterle, Phys. Rev. Lett. **93** 160406 (2004).

[22] J. A. M. Huhtamäki, M. Möttönen, T. Isoshima, V. Pietilä, S. M. M. Virtanen, Phys. Rev. Lett. **97** 110406 (2006).

[23] T. Isoshima, M. Okano, H. Yasuda, K. Kasa, J. A. M. Huhtamäki, M. Kumakura, and Y. Takahashi, Phys. Rev. Lett. **99** 200403 (2007).

[24] T. Ishoshima, J. Phys. Soc. Jpn. **77** 094001 (2008).

[25] T. Kuwamoto, H. Usuda, S.Tojo, and T. Hirano, J. Phys. Soc. Jpn. **79** 034004 (2010).

[26] H. Shibayama, Y. Yasaku, and T. Kuwamoto, J. Phys. B: At. Mol. Opt. Phys. **44** 075302 (2011).

[27] S. Moulder, S. Beattie, R. P. Smith, N. Tammuz, and Z. Hadzibabic, Phys. Rev. A **86** 013629 (2012).

[28] G. Moon, W. J. Kwon, H. Lee and Y. I. Shin, Phys. Rev. A **92** 051601(R) (2015).

[29] C. Raman, J. R. Abo-Shaeer, J. M. Vogels, K. Xu, and W. Ketterle, Phys. Rev. Lett. **87**, 210402 (2001).

[30] E. A. L. Henn, J. A. Seman, G. Roati, K. M. F. Magalhães, and V. S. Bagnato, Phys. Rev. Lett. **103**, 045301 (2009).

[31] E. A. L. Henn, J. A. Seman, G. Roati, K. M. F. Magalhães, and V. S. Bagnato, J. Low Temp. Phys. **158**, 435 (2010).

[32] L. J. LeBlanc, K. Jiménez-García, R. A. Williams, M. C. Beeler, W. D. Phillips and I. B. Spielman, New J. Phys. **17** 065016 (2015).

[33] T. Kuwamoto, private communication.

[34] Y. Kawaguchi, private communication.

[35] E. Torrontegui, S. Ibáñez, S. Martínez-Garaot, M. Modugno, A. del Campo, D. Guéry-Odelin, A. Ruschhaupt, X. Chen, and J. G. Muga, Adv. Atom. Mol. Opt. Phys. **62**, 117 (2013).

[36] M. Demirplak and S. A. Rice, J. Phys. Chem. A **107**, 9937 (2003).

[37] M Berry, J. Phys. A: Math. Gen. **42**, 365303 (2009).

[38] X. Chen, I. Lizuain, A. Ruschhaupt, D. Guéry-Odelin, and J. G. Muga, Phys. Rev. Lett. **105**, 123003 (2010).

[39] M. G. Bason, M. Viteau, N. Malossi, P. Huillery, E. Arimondo, D. Ciampini, R. Fazio, V. Giovannetti, R. Mannella and O. Morsch, Nat. Phys. **8**, 147 (2011).